Conformant Synthesis for Koopman Operator Linearized Control Systems

Niklas Kochdumper, Stanley Bak

***Abstract*— One very promising approach for controlling nonlinear systems is Koopman operator linearization, which approximates nonlinear dynamics with a higher-dimensional linear system. However, since the resulting Koopman linearized model only estimates the actual dynamics, one cannot provide any safety guarantees for the resulting controllers. In this paper we propose a solution to the safety-issue by constructing a Koopman linearized model that is conformant with measurements from the real system using a novel conformant synthesis algorithm that combines trace conformance and reachset conformance. The resulting conformant model can then be used to construct controllers that are safe despite process noise and measurements errors acting on the real system. We demonstrate the superior performance of our conformant synthesis approach compared to previous methods using real data from an electric circuit and a robot manipulator, and we apply our overall framework to safely control a F1tenth racecar.**

***Index Terms*— Conformant synthesis, Koopman operator, control systems, data-driven algorithms.**

I. Introduction

WHILE controlling nonlinear systems is often challenging and computationally demanding, controller design for linear systems is a well-studied problem for which many efficient approaches exist [8], [10], [31], even for high-dimensional systems. This motivates using Koopman operator linearization for control, where the dynamic behavior of a nonlinear system is approximated with a high-dimensional linear system. While the Koopman framework has been successfully applied for many control approaches including model predictive control [19], tracking controllers [11], [33], and linear-quadratic-regulators [5], those controllers are not able to provide any safety guarantees due to the approximative nature of the Koopman linearized model. We address this issue with a novel conformant synthesis approach that adds nondeterminism to the Koopman linearized model to make it conformant with measurements from the real physical system. To obtain a formally safe controller, we can then apply control approaches for linear systems that provide safety guarantees [12], [13], [29] for controller synthesis using the resulting conformant model.

This paragraph of the first footnote will contain the date on which you submitted your paper for review. This work was supported by ??

Niklas Kochdumper and Stanley Bak are both with the Department of Computer Science, Stony Brook University, NY, USA (e-mail: niklas.kochdumper@stonybrook.edu, stanley.bak@stonybrook.edu).

A. Related Work

Koopman operator linearization is based on the Koopman theorem [17], which states that every nonlinear dynamic system can be equivalently represented by an infinite dimensional linear system. Thereby, the state variables of the linear system are defined by so-called *observable functions* or *observables* that represent nonlinear transformations of the original system state. Since it is not possible to compute with infinite dimensions, one in practice selects a finite set of observables yielding an approximative linear system. Many different methods for choosing suitable observables have been proposed: For Carleman linearization [6] the observables are defined by multi-variate monomials. A systematic way to determine appropriate observables are random Fourier features [9], whose usage is motivated by the *Kernel trick*. Moreover, recent approaches also use neural networks as observables [15], [34]. It is also possible to refine a given set of observables based on their closedness under Lie-derivatives to obtain a better approximation [28]. Once the observables are selected, the system matrices of the Koopman linearized system resulting in the best approximation of the original system dynamics can be obtained by applying extended dynamic mode decomposition [32] to measurements or simulations. The Koopman framework is consequently also very well suited for data-driven approaches since the corresponding model can be directly identified from measurements without any need for a symbolic description of the system dynamics in form of a differential equation.

No matter how sophisticated a system model is, the model will never exactly match the behavior of the real physical system. To construct formally safe controllers we therefore require over-approximative models that contain a certain nondeterminism that enables them to enclose all possible behaviors of the real system. The process of checking whether or not a given model is over-approximative is called *conformance testing*, and there exist two main categories of approaches: 1) In *trace conformance* [1], [7] one aims to determine suitable values for the nondeterminism of the model to obtain a system trajectory that is identical with the recorded measurement trace. 2) For *reachset conformance* [3], [27] one checks if the recorded trace is contained in an inner-approximation of the reachable set for the nondeterministic model. An extension to conformance testing is *conformant synthesis*, where the nondeterminism that is required to make the model conformant is determined automatically. Up to now, conformant synthesis approaches have been developed for linear systems [21],

nonlinear systems [3], and hybrid systems [16], all of which are based on reachset conformance.

Some approaches aim to capture the uncertainty for Koopman linearized models by inferring probability distributions over observable functions [14], [23]. Moreover, for Koopman linearized models obtained via Carleman linearization it is possible to compute bounds for the error between the exact dynamics and the Koopman approximation [4], [20]. However, these bounds are usually very conservative. In this paper we present the first conformant synthesis approach for Koopman operator linearized systems, which automatically constructs a tight over-approximative model from measurements of the real physical system using a combination of trace conformance and reachset conformance.

B. Notation

In the remainder of this paper, we will use the following notations: Sets are denoted by calligraphic letters, matrices by uppercase letters, and vectors by lowercase letters. The p-norm of a vector $a \in \mathbb{R}^n$ is denoted by $\|a\|_p$. Given a matrix $A \in \mathbb{R}^{n\times m}$, $A_{(i,\cdot)}$ represents the i-th matrix row, $A_{(\cdot,j)}$ the j-th column, and $A_{(i,j)}$ the j-th entry of matrix row i. The concatenation of two matrices C and D is denoted by $[C\ D]$, and $I_n \in \mathbb{R}^{n\times n}$ is the identity matrix. The symbol $\mathbf{0}$ represents an all-zero matrix of proper dimension, and the empty matrix is denoted by $[\,]$. Given a scalar number $x \in \mathbb{R}$, the floor operator $\lfloor x \rfloor$ rounds to the next lower integer and the signum function $\text{sign}(x)$ returns the sign. Given a set $\mathcal{S} \subset \mathbb{R}^n$, the operator $\texttt{volume}(\mathcal{S})$ returns the volume of the set and the linear map is $M\,\mathcal{S} = \{M\,s \,|\, s \in \mathcal{S}\}$ for $M \in \mathbb{R}^{m\times n}$. Given two sets $\mathcal{S}_1, \mathcal{S}_2 \subset \mathbb{R}^n$, their Minkowski sum is $\mathcal{S}_1 \oplus \mathcal{S}_2 = \{s_1 + s_2 \,|\, s_1 \in \mathcal{S}_1,\, s_2 \in \mathcal{S}_2\}$. We further introduce a zonotope $\mathcal{Z} \subset \mathbb{R}^n$ defined by q generators as $\mathcal{Z} = \{c + \sum_{i=1}^{q} G_{(\cdot,i)}\,\alpha_i \,|\, \alpha_i \in [-1,1]\}$ with $c \in \mathbb{R}^n$, $G \in \mathbb{R}^{n\times q}$ and scalars α_i, for which we use the shorthand $\mathcal{Z} = \langle c, G\rangle_Z$. The zonotope order $\rho = q/n$ represents an estimate for the representation size.

II. Problem Formulation

We consider arbitrary black-box systems with state $x(t) \in \mathbb{R}^n$ and input $u(t) \in \mathbb{R}^m$, where $t \in \mathbb{R}_{\geq 0}$ is the time. A measurement of the system state, which might be subject to a measurement error, is denoted by $\widehat{x}(t)$. A trace of the system consists of a sequence of measurements $\widehat{x}(t_0), \ldots, \widehat{x}(t_s)$ that are obtained when applying the piecewise constant sequence of control inputs $u_1, \ldots, u_s$ to the system. For simplicity, we assume without loss of generality that the measurements are conducted using a fixed sampling rate $\Delta t = t_{i-1} - t_i$, $i = 1, \ldots, s$. Given a list of traces, our goal is to construct a conformant system model that explains all measurements. To achieve this, we first identify a nominal model that approximates the behavior of the black-box system using Koopman operator linearization, which is described in Sec. III. To make this model conformant with the measurements we then add nondeterminism to it, where the required amount of nondeterminism is automatically determined by our novel conformant synthesis algorithm presented in Sec. IV. Several improvements for the algorithm are discussed in Sec. V, before we finally present an extensive experimental evaluation in Sec. VI.

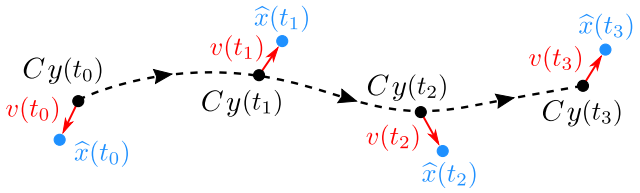

Fig. 1: Schematic visualization of a conformant trajectory.

III. System Identification via Koopman Operator Linearization

Koopman operator linearization introduces a new system state $y(t) = h(x(t)) = [h_1(x(t))\ \ldots\ h_r(x(t))]^T$, which is defined by observable functions $h_j : \mathbb{R}^n \to \mathbb{R}$, $j = 1, \ldots, r$ that represent nonlinear transformations of the original system state $x(t)$. The main idea behind this transformation is that the complex nonlinear dynamic behavior of the original system state $x(t)$ can often be approximated well with a linear system in the higher-dimensional observable space:

$$\begin{aligned} \dot{y}(t) &= A\,y(t) + B\,u(t) \\ x(t) &\approx C\,y(t), \end{aligned} \tag{1}$$

where $y(t_0) = h(x(t_0))$. As described in Sec. I-A, there exist many different approaches to select suitable observables $h(x)$, all of which can be combined with our proposed conformant synthesis approach. Once the observables are fixed, the system matrix $A \in \mathbb{R}^{r\times r}$, the input matrix $B \in \mathbb{R}^{r\times m}$, and the output matrix $C \in \mathbb{R}^{n\times r}$ in (1) resulting in the best approximation of the original system behavior can be computed from the recorded measurement traces by applying a combination of extended dynamic mode decomposition [32] and dynamic mode decomposition with inputs [26]. So overall the Koopman framework generates linear system models that represent accurate approximations of the original system behavior directly from recorded measurement traces, and is therefore well-suited for system identification.

IV. Conformant Synthesis

To construct a conformant model, we extend the Koopman linearized system (1) by nondeterminism in form of a process noise $w(t) \in \mathcal{W}$ and a measurement error $v(t) \in \mathcal{V}$:

$$\begin{aligned} \dot{y}(t) &= A\,y(t) + B\,u(t) + w(t) \\ x(t) &= C\,y(t) + v(t). \end{aligned} \tag{2}$$

The goal of conformant synthesis is to determine minimal sets $\mathcal{W}$ and $\mathcal{V}$ such that the conformant system (2) explains all measurements. Considering a single trace for simplicity, this corresponds to the following optimization problem:

$$\min_{\mathcal{W}\subset\mathbb{R}^r, \mathcal{V}\subset\mathbb{R}^n} \quad \mu\,\texttt{volume}(\mathcal{W}) + (1-\mu)\,\texttt{volume}(\mathcal{V}) \tag{3}$$

subject to

$$y(t_{i+1}) = y(t_i) + \int_0^{\Delta t} A\, y(t) + B\, u_{i+1} + w(t)\ dt \tag{3a}$$

$$\widehat{x}(t_j) = C\, y(t_j) + v(t_j) \tag{3b}$$

$$y(t_0) = h\big(\widehat{x}(t_0) - v(t_0)\big) \tag{3c}$$

$$\forall \tau \in [t_0, t_s]:\ \ w(\tau) \in \mathcal{W} \wedge v(\tau) \in \mathcal{V} \tag{3d}$$

for $i = 0, \dots, s-1$ and $j = 0, \dots, s$, where the user-defined parameter $\mu \in [0, 1]$ can be used to control the relative size of the resulting sets $\mathcal{W}$ and $\mathcal{V}$. The constraint (3a) ensures dynamic feasibility with the model (2), the constraint (3b) connects the actual system state $x(t)$ with the measured state $\widehat{x}(t)$ as visualized in Fig. 1, the constraint (3c) links the original system state $x(t)$ to the state of the Koopman operator linearized system $y(t)$, and the constraint (3d) ensures that the process noise and measurement errors are contained in the corresponding sets. The optimization problem (3) is in general computationally infeasible to solve. We therefore apply several simplifications, which finally enables us to obtain a feasible and close-to-optimal solution for (3) efficiently using trace conformance:

1) We restrict the sets $\mathcal{W}$ and $\mathcal{V}$ to be multi-dimensional intervals.
2) We minimize the norms $\|w(t)\|_1$ and $\|v(t)\|_1$ instead of minimizing the volume.
3) We restrict the functions $w(t)$ and $v(t)$ to be piecewise constant.
4) We set the initial measurement error $v(t_0) = \mathbf{0}$ to zero to avoid the nonlinearity in the constraint (3c).

With these simplifications (3) becomes

$$\min_{\substack{w_1,\dots,w_s \\ v_1,\dots,v_s}} \ \sum_{k=1}^{s} \mu \|w_k\|_1 + (1-\mu)\|v_k\|_1 \tag{4}$$

subject to

$$y(t_{i+1}) = e^{A\Delta t}\, y(t_i) + A^{-1}\big(e^{A\Delta t} - I_r\big)(B\, u_{i+1} + w_{i+1}) \tag{4a}$$

$$\widehat{x}(t_j) = C\, y(t_j) + v_j \tag{4b}$$

$$y(t_0) = h\big(\widehat{x}(t_0)\big) \tag{4c}$$

for $i = 0, \dots, s-1$ and $j = 1, \dots, s$. Note that with suitable slack variables (4) can be formulated as a linear program [30], and therefore be solved very efficiently. Moreover, if the system matrix A is not invertible, we can utilize the power-series of the exponential matrix yielding

$$A^{-1}\big(e^{A\Delta t} - I_r\big) = \sum_{i=1}^{\infty} \frac{1}{i!}\, A^{(i-1)} \Delta t^i.$$

For each measurement trace we obtain a point cloud of optimal values $w_1, \dots, w_s$ and $v_1, \dots, v_s$ for the process noise and measurement errors from (4) as shown in Fig. 2, which we enclose with multi-dimensional intervals to obtain the sets $\mathcal{W}$ and $\mathcal{V}$. The sets $\mathcal{W}$ and $\mathcal{V}$ for multiple measurement traces are finally obtained by computing the union of the intervals for the single traces.

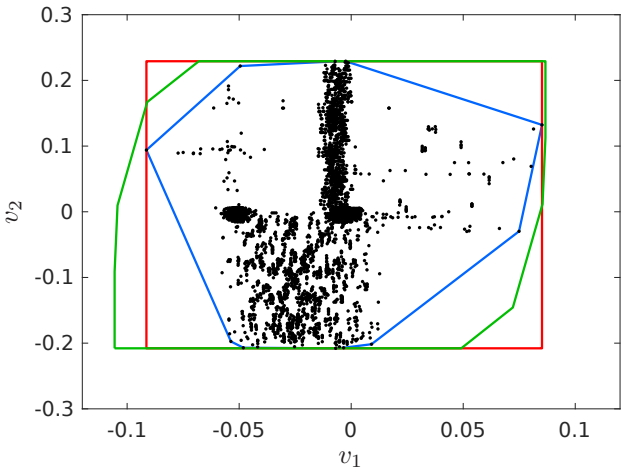

Fig. 2: Enclosure of the point cloud for the measurement error obtained during conformant synthesis of the electric circuit benchmark with an interval (red), a zonotope (green), and a polytope (blue).

V. Improvements

We now presents several improvements to enhance the performance of our conformant synthesis approach.

1) Trace Splitting: One issue we are facing is that the number of measurements s in a trace is often very large in practice. Since the number of variables for (4) is directly proportional to the number of measurements, solving the linear program can therefore be computationally demanding. To circumvent this issue we divide each trace into smaller groups that consist of $d < s$ measurements only. We then solve (4) for each of these groups, where we use the final state $y(t_d)$ from the previous group as the initial state $y(t_0)$ for the next group.

2) Reachset Conformance: After updating the model uncertainty on several traces, many of the remaining traces will already be conformant. This motivates the application of reachset conformance to check if the model is already conformant with a trace, so that we only have to solve the linear program (4) if the check fails. Because reachset conformance is often much faster compared to trace conformance, this significantly reduces the expected runtime for our algorithm. Since the control inputs as well as the process noise are constant during one time step, the reachable set can simply be computed by evaluating (4a) in a set-based manner using zonotopes:

$$\mathcal{R}(t_{i+1}) = e^{A\Delta t}\, \mathcal{R}(t_i) \oplus A^{-1}\big(e^{A\Delta t} - I_r\big)(B\, u_{i+1} + \mathcal{W}),$$

where the initial set is $\mathcal{R}(t_0) = \langle h(\widehat{x}(t_0), [\ ] \rangle_Z$ and set operations on zonotopes are computed according to [18, Sec. I]. Since the Minkowski sum increases the number of zonotope generators in each step, we have to repeatedly reduce the zonotope order if we want to keep the computation time small. While most zonotope order reduction methods compute outer-approximations [18], we require an inner-approximation:

Proposition 1: *(Order Reduction) Given a zonotope $\mathcal{Z} = \langle c, G \rangle_Z \subset \mathbb{R}^n$ and a desired zonotope order $\rho_d \geq 1/n$, the operation* $\texttt{reduce}(\mathcal{Z}, \rho_d) \subseteq \mathcal{Z}$ *returns a zonotope with order smaller than ρ_d that inner-approximates $\mathcal{Z}$:*

$$\texttt{reduce}(\mathcal{Z}, \rho_d) = \big\langle c, [\widetilde{G}\ g] \big\rangle_Z$$

with

$$\widetilde{G} = [G_{(\cdot,o_1)} \ \dots \ G_{(\cdot,o_a)}], \ g = \sum_{i=a+1}^{q} \operatorname{sign}(G_{(1,o_i)})\, G_{(\cdot,o_i)},$$

where $o_1, \dots, o_q$ *are the indices of the sorted generators*

$$\|G_{(\cdot,o_1)}\|_2 \geq \cdots \geq \|G_{(\cdot,o_q)}\|_2$$

and $a = \lfloor \rho_d\, n - 1 \rfloor$ *is the number of unreduced generators.*

Proof. We replace the zonotope

$$\mathcal{Z}_R = \langle \mathbf{0}, [G_{(\cdot,o_{a+1})} \ \dots \ G_{(\cdot,o_q)}] \rangle_Z$$

containing the reduced generators by a zonotope $\mathcal{Z}_U = \langle \mathbf{0}, g \rangle_Z$ consisting of a single generator $g \in \mathbb{R}^n$. Since both vertices g and $-g$ of $\mathcal{Z}_U$ are contained in $\mathcal{Z}_R$ we have $\mathcal{Z}_U \subseteq \mathcal{Z}_R$ since zonotopes are convex, which proves that $\texttt{reduce}(\mathcal{Z}, \rho_d) \subseteq \mathcal{Z}$. The resulting zonotope has order $\rho = (a+1)/n = \lfloor \rho_d \rfloor \leq \rho_d$ and therefore complies with the desired order. □

Checking if a measurement $\widehat{x}(t_i)$ is contained in the reachable set $C\,\mathcal{R}(t_i) \oplus \mathcal{V}$ represented by the Minkowski sum of the zonotope $\mathcal{R}(t_i)$ and the interval $\mathcal{V}$ requires linear programming, which would be computationally too expensive for our purpose. We therefore instead apply a sound but approximative containment check using the following heuristic:

Proposition 2: *(Point Containment) Given a zonotope* $\mathcal{Z} = \langle c, G \rangle_Z \subset \mathbb{R}^n$*, an interval* $\mathcal{I} \subset \mathbb{R}^n$*, and a point* $p \in \mathbb{R}^n$*, it holds that*

$$\big(p - \widetilde{p} \in \mathcal{I}\big) \Rightarrow \big(p \in \mathcal{Z} \oplus \mathcal{I}\big),$$

where

$$\widetilde{p} = c + \sum_{i=1}^{q} \operatorname{sign}\big((p-c)^T G_{(\cdot,i)}\big)\, G_{(\cdot,i)}$$

is an estimate for the point in $\mathcal{Z}$ *that has the smallest distance to* p*.*

Proof. According to the definition of the Minkowski sum we have

$$p = \underbrace{p - \widetilde{p}}_{\in \mathcal{I}} + \underbrace{\widetilde{p}}_{\in \mathcal{Z}} \in \big\{ \underbrace{p - \widetilde{p}}_{\in \mathcal{I}} + \ s_1 \mid s_1 \in \mathcal{Z} \big\}$$
$$\subseteq \big\{ s_1 + s_2 \mid s_1 \in \mathcal{Z}, \ s_2 \in \mathcal{I} \big\} = \mathcal{Z} \oplus \mathcal{I},$$

which proves the proposition. □

If trace splitting is used, one can compute the reachable sets for the single groups to check if a group is already conformant.

3) Set Representations: Using multi-dimensional intervals to represent the sets $\mathcal{W}$ and $\mathcal{V}$ might yield very conservative results, so that a natural idea is to utilize more expressive set representations. The tightest possible convex enclosure can be obtained by computing the convex hull of the point clouds $w_1, \dots, w_s$ and $v_1, \dots, v_s$, which yields polytopes for $\mathcal{W}$ and $\mathcal{V}$. However, convex hull algorithms have exponential complexity with respect to the system dimension [25, Thm. 3.16], which often prevents their application in our case since the observable space is usually high-dimensional. An alternative that often yields a good trade-off between accuracy and compuatation time are zonotopes, where a tight enclosing zonotope for a point cloud can be computed using the algorithm in [22, Sec. VI.B]. An example for the enclosure of a point cloud with different set representations is shown in Fig. 2.

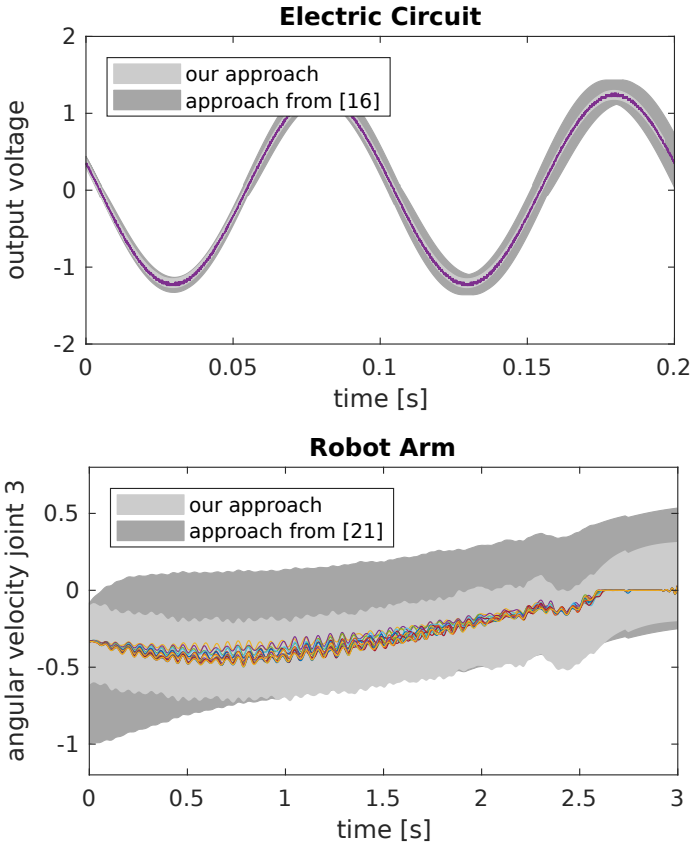

Fig. 3: Comparison of the reachable sets for selected measurement traces corresponding to conformant models constructed using different conformant synthesis approaches, where the results for the approach from [16] are taken from [16, Fig. 7] and the results for the approach from [21] are taken from [21, Fig. 4].

VI. Experiments

We now demonstrate the performance of our novel conformant synthesis algorithm on several benchmark systems. In particular, we consider a dataset from an electric circuit that represents a LMC6484 lowpass filter consisting of 6 measurement traces [16], a dataset from a 6 degree-of-freedom Schunk LWA 4P robot arm consisting of 2055 measurement traces [21], and a dataset from a F1tenth racecar [24] consisting of 41 measurement traces. The electric circuit has 3 states and a single input, where the states are the output voltage and two internal voltages, and the input is the input voltage to the circuit. The robot arm has 12 states and 6 inputs, where the states are the angles and angular velocities for each of the 6 joints, and the inputs are the torques of the joint motors. The F1tenth car has 4 states and 2 inputs, where the states are the x- and y-position of the cars center, the orientation of the car, and the cars velocity, and the inputs are the desired steering angle and the desired velocity. The sampling rate is $\Delta t = 8\mu s$ for the electric circuit, $\Delta t = 4ms$ for the robot arm, and $\Delta t = 25ms$ for the F1tenth racecar. We implemented our

Tab. 1: Comparison of the resulting conformant Koopman linearized models for different types of observables with respect to the average relative simulation error for the nominal model, the average volume of the tightest interval enclosing the reachable set for the conformant model, and the average computation time of conformant synthesis for one second of data. In addition, the trade-off parameters μ used for conformant synthesis are listed.

Benchmark	**Random Fourier Features**				**Neural Network Observables**			
	μ	avg. rel. sim. error	avg. volume	comp. time / s	μ	avg. rel. sim. error	avg. volume	comp. time / s
Electric Circuit	0.5	6.77%	$8.79 \cdot 10^{-3}$	2.06s	0.5	6.38%	$1.01 \cdot 10^{-2}$	1.95s
Robot Arm	0.5	5.08%	$1.19 \cdot 10^{-2}$	0.02s	0.9	6.91%	$4.31 \cdot 10^{-2}$	0.02s
F1tenth Racecar	0.5	6.53%	$1.79 \cdot 10^{-3}$	0.03s	0.5	6.42%	$1.16 \cdot 10^{-3}$	0.02s

conformant synthesis approach in MATLAB, and we use the toolbox CORA [2] for reachability analysis. All computations are carried out on a 2.9GHz quad-core i7 processor with 32GB memory.

A. Different Types of Observables

As described earlier in Sec. I-A, there exist many different methods to determine suitable observables for Koopman operator linearization. To demonstrate that our conformant synthesis algorithm works well for arbitrary types of observables, we compare its performance for random Fourier feature observables [9] and neural network observables [15]. For fairness we use $r = 100$ observables, a group size of $d = 5$ for trace splitting, as well as a desired zonotope order of $\rho_d = 5$ in both cases, and we represent the sets $\mathcal{W}$ and $\mathcal{V}$ by intervals. The corresponding results for the different benchmark systems are summarized in Tab. 1. Both Koopman linearized models achieve a similarly good accuracy, which can be deduced from the small relative error between simulations of the nominal model and the recorded measurement traces. Moreover, the consistently small volume of the reachable set for the conformant models indicates that our conformant synthesis algorithm performs equally well for different types of observables. Finally, for all but the very high-frequency sampled electric circuit benchmark, the computation time of our conformant synthesis algorithm for one second of data is smaller than one second, so that our algorithm is actually real-time capable for most systems.

B. Comparison with other Approaches

We now compare our approach for conformant synthesis with other state of the art methods. For fairness we consider the original results published in the corresponding papers for the other methods to avoid a biased evaluation due to badly tuned algorithm parameters. In particular, this means that we compare to the conformant synthesis algorithm for hybrid systems [16] using the electric circuit benchmark, and to the conformant synthesis algorithm for linear systems [21] using the robot arm benchmark. For both benchmarks we use the conformant model constructed with random Fourier features for our approach. As shown in Fig. 3, for both benchmarks our conformant synthesis algorithm yields a tighter reachable set than previous methods, which can be attributed to the fact that our approach constructs a more accurate conformant model.

C. Formally Safe Controller Synthesis

One of the main applications for our conformant synthesis approach is the design of formally safe controllers. We therefore now use the conformant model for the F1tenth car corresponding to the random Fourier feature observables to construct a safe controller for solving a typical reach-avoid problem. In particular, we use a model predictive control approach similar to the one in [13], which directly optimizes over reachable sets to determine the optimal control inputs. This also highlights one of the biggest advantages of our Koopman-based conformance approach: While reachability analysis for nonlinear vehicle models is in general too slow to execute the optimization over reachable sets required for model predictive control during online application, reachability analysis for the conformant linear Koopman model is fast enough for real-time capability. In addition, for the linear Koopman model one can exploit the superposition principal to pre-compute the reachable set due to the process noise $w(t) \in \mathcal{W}$ offline, which further accelerates the computations. For online control we implemented a ROS node using Python, and we apply the sequential least squares programming algorithm from the SciPy package[1] to solve the optimization problem for model predictive control. Moreover, identically to the setup used to obtain the F1tenth dataset, the x- and y-positions as well as the orientation of the car are determined from lidar measurements and the cars velocity is calculated based on the measured motor speed. The results shown in Fig. 4 demonstrate that the we can successfully control the car with the conformant Koopman linearized model so that it safely reaches the goal set while avoiding the obstacle.

VII. Conclusion

In this work we introduced the first conformant synthesis approach for Koopman operator linearized control systems. Our method addresses one of the biggest disadvantages of the Koopman framework, which is the lack of safety guarantees due to the approximative nature of the resulting linear Koopman models. With the conformant Koopman models constructed by our approach it is now possible to control complex dynamical systems using efficient techniques for linear systems in a formally safe manner, as we demonstrate on the example of a F1tenth racecar. Finally, since our approach

[1] https://scipy.org/

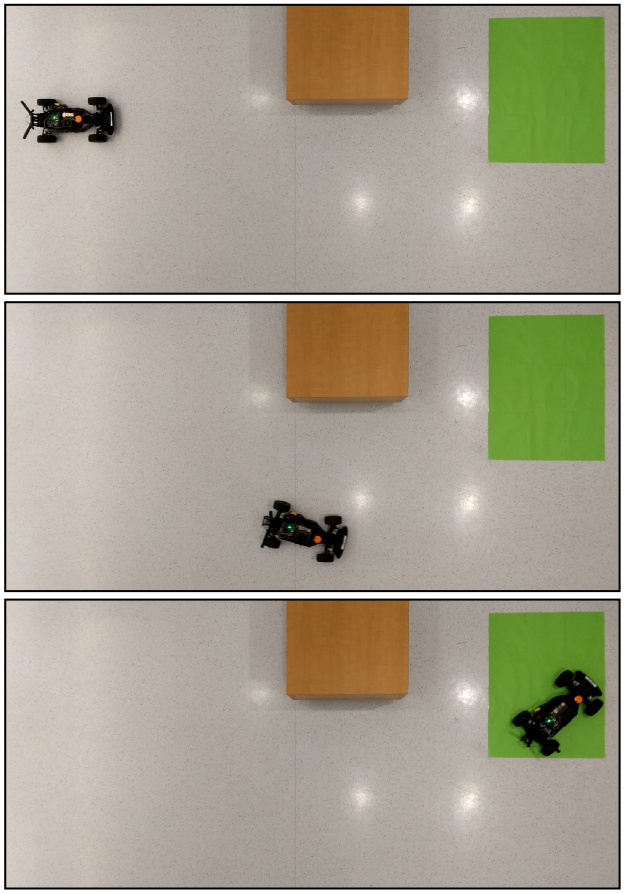

Fig. 4: Position of the F1tenth racecar at times 0s, 4.9s, and 9.8s during online application of model predictive control, where the goal set is shown in green and the obstacle is shown in orange.

combines the precision of trace conformance with the computational efficiency of reachset conformance, it is for many systems faster than real-time while still being more accurate than previous methods.

References

[1] H. Abbas, H. Mittelmann, and G. Fainekos. Formal property verification in a conformance testing framework. In *Proc. of the Int. Conference on Formal Methods and Models for Co-Design*, pages 155–164, 2014.

[2] M. Althoff. An introduction to CORA 2015. In *Proc. of the Int. Workshop on Applied Verification for Continuous and Hybrid Systems*, pages 120–151, 2015.

[3] M. Althoff and J. M. Dolan. Reachability computation of low-order models for the safety verification of high-order road vehicle models. In *Proc. of the American Control Conference*, pages 3559–3566, 2012.

[4] A. Amini, Q. Sun, and N. Motee. Error bounds for Carleman linearization of general nonlinear systems. In *Proc. of the Int. Conference on Control and its Applications*, pages 1–8, 2021.

[5] S. L. Brunton, B. W. Brunton, J. L. Proctor, and J. N. Kutz. Koopman invariant subspaces and finite linear representations of nonlinear dynamical systems for control. *PLOS ONE*, 11(2):1–19, 2016.

[6] T Carleman. Application de la théorie des équations intégrales linéaires aux systèmes d'équations différentielles non linéaires. *Acta Mathematica*, 59:63–87, 1932.

[7] T. Dang. Model-based testing of hybrid systems. In *Model-Based Testing for Embedded Systems*, pages 411–452. Taylor & Francis, 2017.

[8] P. De Larminat. *Analysis and control of linear systems*. John Wiley & Sons, 2013.

[9] A. M. DeGennaro and N. M. Urban. Scalable extended dynamic mode decomposition using random kernel approximation. *SIAM Journal on Scientific Computing*, 41(3):1482–1499, 2019.

[10] F. W. Fairman. *Linear control theory: The state space approach*. John Wiley & Sons, 1998.

[11] C. Folkestad, S. X. Wei, and J. W. Burdick. Quadrotor trajectory tracking with learned dynamics: Joint Koopman-based learning of system models and function dictionaries. *arXiv preprint arXiv:2110.10341*, 2021.

[12] F. A. C. C. Fontes, S. V. Raković, and I. V. Kolmanovsky. Rigid tube model predictive control for linear sampled–data systems. In *Proc. of the IFAC World Congress*, pages 9840–9845, 2017.

[13] F. Gruber and M. Althoff. Scalable robust model predictive control for linear sampled-data systems. In *Proc. of the Int. Conference on Decision and Control*, pages 438–444, 2019.

[14] Minghao Han, Jacob Euler-Rolle, and Robert K. Katzschmann. DeSKO: Stability-assured robust control with a deep stochastic Koopman operator. In *Proc. of the Int. Conference on Learning Representations*, 2022.

[15] Y. Han, W. Hao, and U. Vaidya. Deep learning of Koopman representation for control. In *Proc. of the Int. Conference on Decision and Control*, pages 1890–1895, 2020.

[16] N. Kochdumper, A. Tarraf, M. Rechmal, M. Olbrich, L. Hedrich, and M. Althoff. Establishing reachset conformance for the formal analysis of analog circuits. In *Proc. of the Asia and South Pacific Design Automation Conference*, pages 199–204, 2020.

[17] B. O. Koopman. Hamiltonian systems and transformation in Hilbert space. *Proceedings of the National Academy of Sciences of the United States of America*, 17(5):315–318, 1931.

[18] A.-K. Kopetzki, B. Schürmann, and M. Althoff. Methods for order reduction of zonotopes. In *Proc. of the Int. Conference on Decision and Control*, pages 5626–5633, 2017.

[19] Milan Korda and Igor Mezić. Linear predictors for nonlinear dynamical systems: Koopman operator meets model predictive control. *Automatica*, 93:149–160, 2018.

[20] J.-P. Liu, H. Ø. Kolden, H. K. Krovi, N. F. Loureiro, K. Trivisa, and A. M. Childs. Efficient quantum algorithm for dissipative nonlinear differential equations. *Proceedings of the National Academy of Sciences of the United States of America*, 118(35), 2021.

[21] S. B. Liu and M. Althoff. Reachset conformance of forward dynamic models for the formal analysis of robots. In *Proc. of the Int. Conference on Intelligent Robots and Systems*, pages 370–376, 2018.

[22] M. Maïga, N. Ramdani, L. Travé-Massuyè, and C. Combastel. A comprehensive method for reachability analysis of uncertain nonlinear hybrid systems. *Transactions on Automatic Control*, 61(9):2341–2356, 2015.

[23] J. Morton, F. D. Witherden, and M. J. Kochenderfer. Deep variational Koopman models: Inferring Koopman observations for uncertainty-aware dynamics modeling and control. In *Proc. of the Int. Joint Conference on Artificial Intelligence*, pages 3173–3179, 2019.

[24] M. O'Kelly, H. Zheng, D. Karthik, and R. Mangharam. F1tenth: An open-source evaluation environment for continuous control and reinforcement learning. *Proceedings of Machine Learning Research*, 123:77–89, 2020.

[25] F. P. Preparata and M. I. Shamos. *Computational Geometry: An Introduction*. Springer Science & Business Media, 2012.

[26] J. L. Proctor, S. L. Brunton, and J. N. Kutz. Including inputs and control within equation-free architectures for complex systems. *The European Physical Journal Special Topics*, 225(13):2413–2434, 2016.

[27] H. Roehm, J. Oehlerking, M. Woehrle, and M. Althoff. Reachset conformance testing of hybrid automata. In *Proc. of the Int. Conference on Hybrid Systems: Computation and Control*, pages 277–286, 2016.

[28] S. Sankaranarayanan. Automatic abstraction of non-linear systems using change of bases transformations. In *Proc. of the Int. Conference on Hybrid Systems: Computation and Control*, pages 143–152, 2011.

[29] B. Schürmann and M. Althoff. Optimal control of sets of solutions to formally guarantee constraints of disturbed linear systems. In *Proc. of the American Control Conference*, pages 2522–2529, 2017.

[30] A. M. Tillmann. Equivalence of linear programming and basis pursuit. *Proceedings in Applied Mathematics and Mechanics*, 15(1), 2015.

[31] H. L. Trentelman, A. A. Stoorvogel, and M. Hautus. *Control theory for linear systems*. Springer Science & Business Media, 2012.

[32] M. O. Williams, I. G. Kevrekidis, and C. W. Rowley. A data–driven approximation of the Koopman operator: Extending dynamic mode decomposition. *Journal of Nonlinear Science*, 25(6):1307–1346, 2015.

[33] Y. Xiao. DDK: A deep Koopman approach for dynamics modeling and trajectory tracking of autonomous vehicles. *arXiv preprint arXiv:2110.14700*, 2021.

[34] E. Yeung, S. Kundu, and N. Hodas. Learning deep neural network representations for Koopman operators of nonlinear dynamical systems. In *Proc. of the American Control Conference*, pages 4832–4839, 2019.